Pacific Northwest
NATIONAL LABORATORY

PNNL-32738

Stable Catalysts for Combined Dry and Steam Reforming of Methane and Carbon Dioxide

March 2022

Mond F. Guo
Gregory B. Collinge
Sarah I Allec
Roger J. Rousseau
Casper O. Brady
Huamin Wang
Jonathan L. Male

U.S. DEPARTMENT OF ENERGY

Prepared for the U.S. Department of Energy
under Contract DE-AC05-76RL01830

DISCLAIMER

PACIFIC NORTHWEST NATIONAL LABORATORY
operated by
BATTELLE
for the
UNITED STATES DEPARTMENT OF ENERGY
under Contract DE-AC05-76RL01830

Printed in the United States of America

Available to DOE and DOE contractors from the Office of Scientific and Technical Information,
P.O. Box 62, Oak Ridge, TN 37831-0062
www.osti.gov
ph: (865) 576-8401
fax: (865) 576-5728
email: reports@osti.gov

Available to the public from the National Technical Information Service
5301 Shawnee Rd., Alexandria, VA 22312
ph: (800) 553-NTIS (6847)
or (703) 605-6000
email: info@ntis.gov
Online ordering: http://www.ntis.gov

PNNL-32738

Stable Catalysts for Combined Dry and Steam Reforming of Methane and Carbon Dioxide

March 2022

Mond F. Guo
Gregory B. Collinge
Sarah I Allec
Roger J. Rousseau
Casper O. Brady
Huamin Wang
Jonathan L. Male

Prepared for
the U.S. Department of Energy
under Contract DE-AC05-76RL01830

Pacific Northwest National Laboratory
Richland, Washington 99354

Short Description

The specific aim of this project is to develop a comprehensive understanding of cheaper and more stable methane and carbon dioxide reforming catalysts with an optimal introduction of steam to reduce catalyst deactivation due to carbon deposits that typically prevent the catalytic systems from transferring to commercial implementation. The work was proposed as a two-year project with the end goal of showing a reliable catalyst system run for at least 400 hours at temperatures less than 800 °C with less than 5% loss of activity of the catalyst and a carbon monoxide to hydrogen product ratio of at least 1:1. The project went for one-year and met the end of year milestone by developing two strategies (use of a cerium co-catalyst and introducing 5% water) that reduced the carbon deposition rates by at least 20% relative to the baseline 10% Ni MgAlO methane reforming of CO_2 at < 800 °C in order to show technical feasibility of the concept.

Mission Relevance

All of the Department of Energy (DOE) is interested in science and innovation to reduce the carbon-intensity of the industry and transportation sectors; scientific breakthroughs need to be understood at the molecular level to drive optimization (Basic Energy Sciences); Fossil Energy and Carbon Management, and Energy Efficiency and Renewable Energy are interested in reliable catalytic systems that are efficient with their use of carbon dioxide and methane from various sources. A successful outcome from this project will contribute to catalyzing the timely, material, and efficient transformation of the nation's energy systems. While DOE is currently not funding the area of advanced gasification[1] coupled to CO_2 utilization, it will clearly benefit from a fundamental understanding of this research area as well as the many sources of distributed methane and CO_2.

Specific Aims

In the energy future, there will be a need to use both methane and carbon dioxide emissions in a more environmentally positive manner. One such example of both emissions is biogas which is typically 50-60% methane and 50-40% carbon dioxide, which is produced from anaerobic digestion of waste carbon. Steam Reforming of Methane (SRM) is used commercially today to produce carbon monoxide and hydrogen (synthesis gas) in a ratio of typically 1:3, respectively. However, it does not use carbon dioxide as a reactant. There has been extensive research on Dry Methane and carbon dioxide Reforming (DMR), which apparently uses both methane and carbon dioxide as reactants and produce synthesis gas with a carbon monoxide to hydrogen ratio of 1:1. This ratio is capable of readily being converted to methanol or acetic acid. However, key challenges preventing the technology from going to market have been the use of platinum group metals at higher reaction temperatures (> 800 °C) and the rapid deactivation of catalysts due to carbon depositions via the Boudouard reaction, methane decomposition, and the reverse carbon gasification reaction—all together with the formation of metal carbides.

There is an opportunity to utilize potentially cheaper nickel catalysts at lower reaction temperatures (500-775 °C) with significant challenges currently around carbon deposits

and aggregation of small nanoparticles. The design of the catalyst may be enhanced for better dispersion of nickel, which are advantageous to reducing coke formation, by including lower levels of co-catalysts (such as tin, iron, lanthanum) to maximize interaction with the support, and by tuning the basicity of the catalyst system (introduce magnesia into the alumina support) to enable activity and resilience. Furthermore, steam will be deliberately introduced into the system to convert the carbon deposits back to carbon monoxide while maintaining the stability of the catalysts and target the approximately 1:1 – 1:2 ratio of carbon monoxide to hydrogen for subsequent conversion to oxygenated molecules.

In terms of perturbing the system equilibria by steam in the complex molecular system of forward and reverse reactions, thermodynamic and kinetic simulations based on experimental parameterizations show that while excess H_2O mitigates coke formation, it comes at the cost of CO_2 conversion as DMR is circumvented in favor of Steam Reforming of Methane. Molecularly speaking, carbon deposition is suggested to be most sensitive to the formation and ability of hydroxyls to oxidize carbon deposits, making a careful control over the chemical equilibria responsible for hydroxyl formation necessary. It is hypothesized that catalyst deactivation can be mitigated by choosing a catalyst and steam co-feed ratio that maximizes the decoupling of oxidant formation equilibria from those equilibria responsible for DRM, allowing us to disrupt/enhance oxidant formation without sacrificing DRM activity. The proposed work will be both experimental and theoretical to model and scientifically understand the numerous complex and competing reactions proceeding on catalyst surfaces and build kinetic models coupled to reactor models to predict performance.

Background and Significance

Understanding the kinetics and interaction of the reactions of carbon dioxide, carbon monoxide, water, methane, and the forms of carbon deposits on the surface of the catalyst are vital to combating deactivation reactions and obtaining maximal efficiency for the production of synthesis gas from waste carbon dioxide and methane. Along with the understanding of the kinetics and molecular modeling of the system, there will be opportunity to apply the understanding to arrive at optimal solutions for molecular- and energy-efficiency. Additionally, understanding the molecular structure and dispersion of the metal catalyst on the support through tuning of the basicity of the support,[2,3] and co-catalysts to stabilize the dispersed metal active sites,[4-6] and prevent occlusion with different forms of carbon deposits[8-10] or reaction with additional amounts of water[11-13]; is the best way to have science inform the development of a stable catalyst.

An activity-structure relationship will be developed both experimentally and theoretically to develop nickel catalysts that are molecularly controlled to be of the optimal dispersion and stability in the presence of carbon and metal oxide forming conditions. To address the need for a robust, accurate modeling tool, a microkinetics-based simulation program that describes the reactions taking place on the surface of a catalyst will be developed.[14] Microkinetic modeling was advocated as a suitable approach, which covers different scales and dynamically evolving extents of reaction, to optimize both the processes for the catalytic oxidation and reforming of methane.[11] It has been shown that dry methane reforming can have carbon deposits being inhibited by both hydrogen

and water. However, water provided a better inhibition effect than does hydrogen on a Ni/Al_2O_3 catalyst.[11] There is very little published on long term stability (200 hours) of carbon dioxide methane reforming nickel catalysts[8] and this is vital to enable transition to market. Understanding how the introduction of minimal additional water into the system and optimization for maximum performance and stability is yet to be attained. *We thus hypothesize that catalyst deactivation can be mitigated by choosing a catalyst and steam co-feed ratio that maximizes the decoupling of oxidant formation equilibria from those equilibria responsible for carbon dioxide reforming of methane, allowing us to disrupt/enhance oxidant formation without sacrificing carbon dioxide reforming of methane activity.*

Research Design and Methodology

Research developed during this project will advance the understanding of carbon dioxide utilization through reforming with methane and the minimum amount of additional water needed to ensure a stable catalyst. A detailed understanding of the control of catalyst and co-catalyst on support as well as how carbon deposits are formed will be developed. Control of the molecular dispersion of the catalysts and their interaction with the co-catalyst and support will be vital to enabling the oxidation of carbon while maintaining reduced and dispersed nickel sites. The project will culminate with an extended run of 400 hours with less than 5% loss of activity for the methane reforming of CO_2. With the large number of molecular interactions occurring between the catalytic system, reactants, and products, modeling will be essential in guiding experiments and helping to explain unexpected results. Models will be developed and verified with carefully designed experiments such that models may ultimately simulate reaction systems and enhance the probability of experimental success with theory driving scientific understanding.

FY 2021 Plan

In the first year of this project, research will advance the understanding of nickel catalytic systems that are resilient to carbon deposition and changes to the nickel species in the presence of additional water.

Task 1: Developing a structure-property relationship of the nickel catalyst system for methane reforming of carbon dioxide

1.1 The introduction of magnesia into the alumina to alter the acid-base properties of the support to reduce carbon deposit formation, increase stability of the Ni site, control the molecular size of the Ni site.

The baseline system will be 10% nickel on alumina. With the first system to investigate being 10% Ni in a $Ni/MgAl_2O_4$ spinel,[15] and/or a Ni/MgAl(O) derived from a hydrotalcite-like derivative.[17]). Materials will be calcined at 900 °C to ensure when testing at 650, 700, 750 and 800 °C that the structure is unaltered due to heating, with the lower temperatures utilized to ensure some coke formation. The CH_4: CO_2 ratio will be maintained at 1:1 and the highest space velocity used to ensure maximum conversion, use all the active sites, and see carbon deposition.

1.2 The use of co-catalysts to stabilize the Ni and control the Nickel dispersion. Co-Catalysts will be added to the Nickel catalyst system to stabilize and enhance the dispersion to increase the prevalence of smaller sized nickel particles and to enhance the uptake of CO_2, such as: La ,[6,17] Sn,[5] and Fe.[4]

The controlled reaction of dilute gaseous reactants to gather the kinetics of the system in order that the process can be understood and scale-up enabled. Such information can be used to effectively benchmark the kinetic models to be developed in Task 3, increasing the model's tangency to reality and ensuring it provides both efficacious kinetic predictions as well as molecular-level insights.

Task 2: Understand the mechanism of formation of carbon deposits on the nickel catalysts and the Deactivation mechanisms of Nickel
Temperature Programmed Oxidation, Raman Spectroscopy, X-ray Photoelectron Spectroscopy, Scanning Electron Microscopy, and Tunnelling Electron Microscopy will be used after reaction to examine the form and relative amounts of carbon nanotubes and graphite fibers deposited on the catalyst.[6,8] Leveraging task 1.2 it will be important to understand the effects of co-catalysts on carbon deposition reactions.

Task 3: Simulation of the complex catalytic system
In this task, thermodynamic properties from nickel systems on alumina and nickel with MgAl(O) will be leveraged to build preliminary models using the thermodynamics of the reactions occurring on nickel and alumina, how the carbon grows, the effects of increased steam on carbon deposition, the $CO:CO_2:CH_4$ ratio, the stability of the Nickel catalyst, and the resultant the $CO:H_2$ ratio.[7, 11-13]

FY 2022 Projected Scope

Systematic introduction of additional water into the best Ni catalyst systems. It has been shown that water can inhibit the carbon formation more than hydrogen.[7,11-13] Additional work will be done to ensure the nickel-based catalysts is also stable to the presence of additional water and does not oxidize or change particle size.

Technical Milestones

- Develop an initial thermodynamics-based model of the carbon deposition reactions on the Nickel on alumina and Magnesium Aluminate (August 2021)
- Distribute, characterize, and control the nickel particle size on MgAl(O) (July 2021)
- Develop a detailed understanding of the carbon deposition on MgAl(O) and have at least two strategies to help abate the issue, such as but not limited to, catalysts preparation, introduction of a co-catalyst etc. (September 2021)
- Show technical feasibility of a nickel catalyst system with additional minimal amounts of water (March 2022)
- Develop kinetic model of nickel catalyst system for the methane reforming of CO_2 with minimal amounts of water (June 2022)

- By end of year show two strategies (cocatalysts, with and without water) that reduce the carbon deposition rates by 20% relative to the baseline Ni MgAlO at < 800 °C. This means at 650-750 °C that the technical feasibility of concept is shown. (September 2022).

Plan Executed in FY 2021

Task 1 Developing a structure-property relationship of the nickel catalyst system for methane reforming of carbon dioxide
and

Task 2: Understand the mechanism of formation of carbon deposits on the nickel catalysts and Deactivation mechanisms of Nickel

Catalyst synthesis and characterization
Robert Dagle and Vanessa Dagle had previously worked on methane steam reforming over $MgAl_2O_4$ – supported rhodium and iridium catalysts and used Puralox 30/140 from Sasol[16] (which is 30% MgO and 70% Al_2O_3 with a nominal surface area of 140 m^2/g after a treatment at 550 °C in air; denoted at MG30) and very kindly provided some to the project. The Puralox 30/40 was calcined at 550 °C in air and then wet impregnated with 10 wt% Ni and calcined with at heating ramp rate of 10 °C/min up to 900 °C and held for at least 4 hours in air.

Table 1. The Brunauer-Emmett-Teller (BET) surface area analysis of support and the first catalyst

Samples	1	2	3	4
	MG30-uncalcined	MG30-550C	MG30-900C	10%Ni-MG30-900C
Surface area(m^2/g)	136.9	191.1	85.6	77.9
Total Volume (cc/g)	0.28	0.43	0.36	0.29

The samples were degassed at 150 °C for 4 hours before measurement.

The surface area of the support is seen to be reduced significantly upon increasing calcination from 550 to 900 °C (Table 1). The support alone and the support with 10 wt% Ni when both calcined at 900 °C have similar surface areas and total pore volume with the sample with 10wt% Ni has a slightly smaller value.

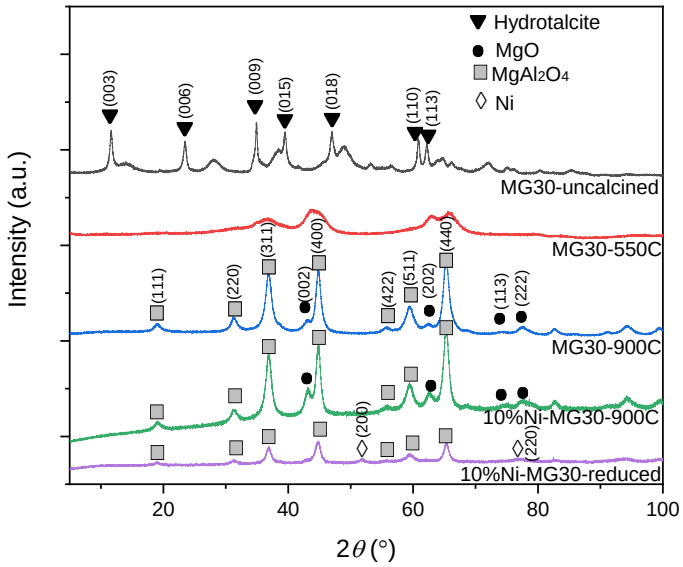

Figure 1. The powder X-ray diffraction patterns of the 10 wt% Ni $MgAlO_x$ catalyst and controls:

The powder X-ray diffraction of the sample of the reduced 10% Ni on $Mg_2Al_2O_4$ was obtained by passivating the surface of the Ni metal with 0.5% in N_2 to form a thin oxide layer. In Figure 1 the MG30 hydrotalcite precursor goes to an amorphous Mg-Al-Ox at a lower calcination temperature and ultimately forms a $MgAl_2O_4$ spinel at a calcination temperature of 900 °C with a little excess MgO. When the 10% Ni $Mg_2Al_2O_4$ sample is reduced under hydrogen no crystalline $Ni_xMg_{(1-x)}Al_2O_4$ or NiO is seen and only a well dispersed Ni metal phase is observed.

In addition to the baseline 10%Ni/MgAlOx catalyst, three more catalysts, 5%Ni/MgAlOx, 5%Ni5%Ce/MgAlOx, and 5%Ni5%Co/MgAlOx, have been synthesized and their BET surface area and XRD patterns are reported in Table 2 and Figure 2, respectively. All these materials were made by wet impregnation of the same support. All the catalysts were calcined to 900 °C. The hypothesis was the surface areas would be very similar, at this time it is especially perturbing as to why the 5% Ni/ $MgAlO_x$ has a smaller surface area than the 10%Ni/$MgAlO_x$. The XRD results did not much difference, suggesting these samples contains $MgAl_2O_4$ spinel support and well dispersion Ni, NiCe, or NiCo metallic phases. CO Chemisorption of the Ni catalysts used in this study were conducted after the pretreatment of the catalysts with H_2 at 280 °C for 30 minutes. The results in Table 3 showed that CO chemisorption depends on Ni loading.

Table 2. The Brunauer-Emmett-Teller (BET) surface area analysis of the Ni catalysts was used in this study.

Samples	5%Ni/ MG30	10%Ni/ MG30	5%Ni5%Ce/ MG30	5%Ni5%Co/ MG30
Surface area (m2/g)	56.1	75.7	88.4	69.6

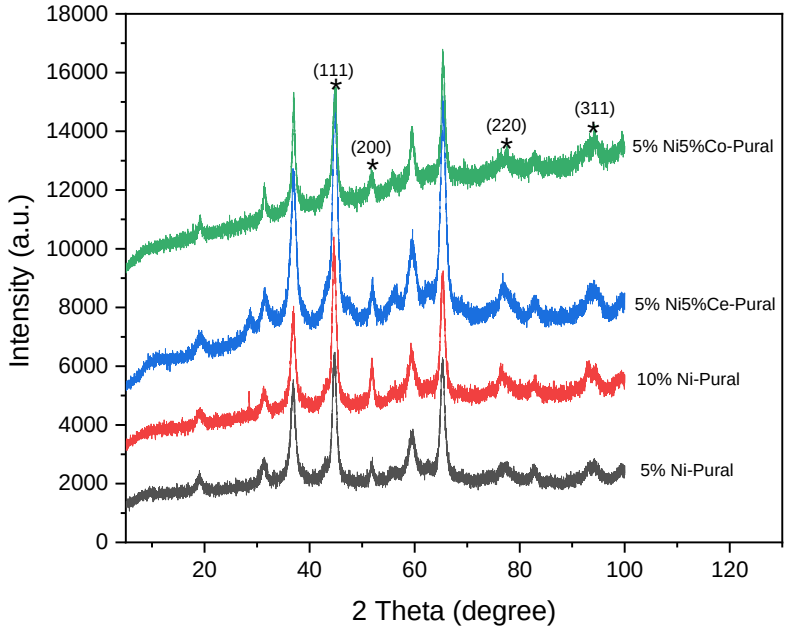

Figure 2 The powder X-ray diffraction patterns of the 10 wt% Ni/$MgAlO_x$, 5 wt% Ni/$MgAlO_x$, 5 wt% Ni-5wt% Co/$MgAlO_x$, 5 wt% Ni-5wt% Ce/$MgAlO_x$ catalysts.

Table 3. CO Chemisorption of the Ni catalysts used in this study.

Samples	5% Ni/$MgAlO_x$	10% Ni/$MgAlO_x$	5%Ni5%Co /$MgAlO_x$	5%Ni5%Ce /$MgAlO_x$
Cumulative Quantity (μmol/g)	5.36	24.94	12.55	10.75

Catalyst testing for methane reforming of carbon dioxide

Testing the base-line catalyst

The catalysts were diluted with α-Al_2O_3 calcined to 1000 °C for 4 hours, diluent:catalyst 5:1, to help with gas mixing and reduction of localized exotherms. Reduction of the 10% Ni/$MgAlO_x$ 150-500 micron particle size catalyst was carried out at 850 °C for 30 minutes under 10% H_2 in He with a ramp rate of 10 °C/min and a flow rate of 1 mL/s. After 30 minutes at 850 °C the catalyst was switched to He. As shown in Figure 3, H_2 consumption peaks were observed at around 650 -850 °C, suggesting most of the Ni interacts strongly with the support after calcination.

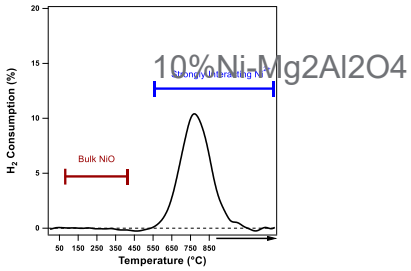

Figure 3. Reduction of 10% Ni $Mg_2Al_2O_4$ under 10% H_2 at up to 850 °C

Reaction conditions were with 30 mg of catalyst, space velocity 80 L g^{-1} h^{-1}, CO_2:CH_4 of 1:1 with helium as the diluent, at 750, 700, 650, 800, and 750 °C. The second test at 750 °C was to examine any permanent changes to the catalyst during the experiment.

Figure 4 showed the 10%Ni $Mg_2Al_2O_4$ catalyst activity and stability at 650, 700, and 750 °C, and 1:1 CO_2:CH_4. There is less than equilibrium conversion in all three temperatures. Carbon balances are all between 98 and 105% for all time on stream.

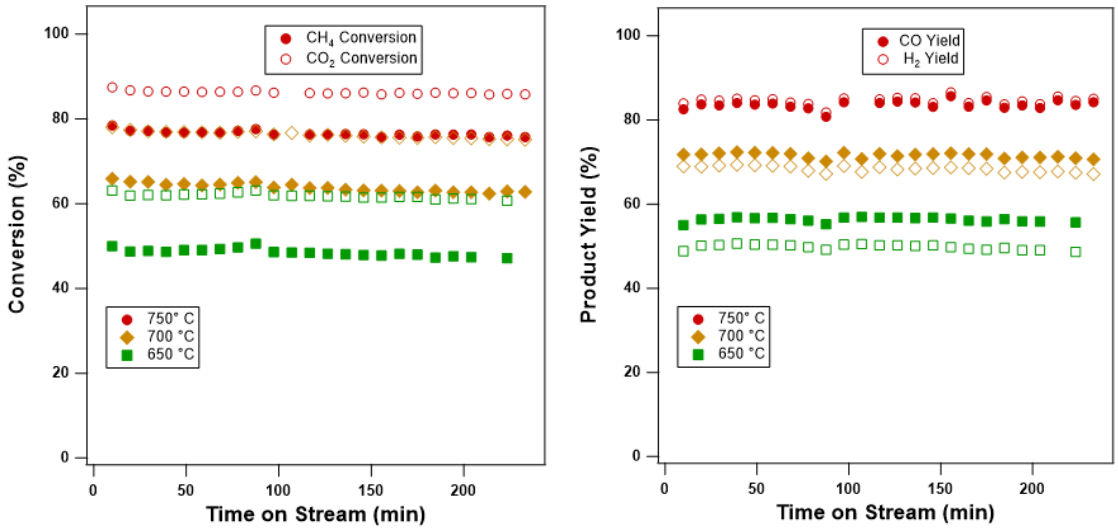

Figure 4. 10%Ni $Mg_2Al_2O_4$ catalyst conversion of CO_2 and CH_4 and production of H_2 and CO at 650, 700, and 750 °C.

Figure 5 shows the normalized CH_4 conversion at the different reaction temperature to indicate the catalyst deactivation rate. There is some deactivation, and we can obtain approximate deactivation rates, 650 > 700 > 750 °C, however, 800 °C seems to deactivate faster than 750 °C which could be a faster sintering rate of the Ni because

the carbon deposits are so small at 800 °C. At the lower temperatures, we expect more carbon deposition.

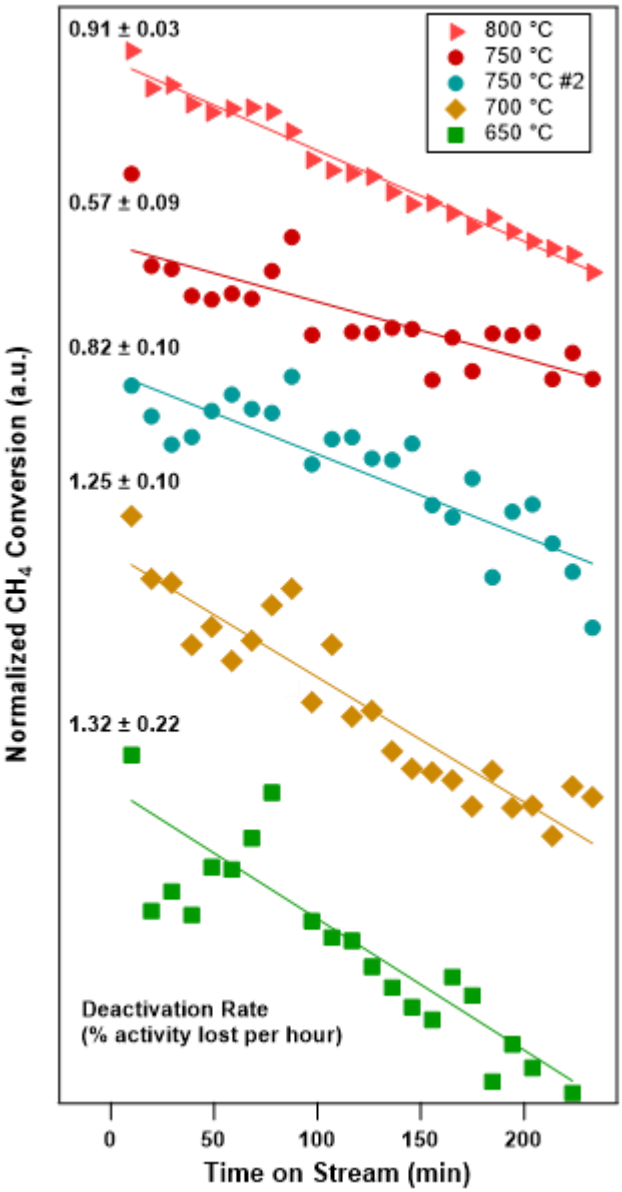

Figure 5. 10%Ni $Mg_2Al_2O_4$ normalized CH_4 conversion as an indicator of catalyst deactivation at 750, 700, 650, 800, and 750 °C.

After the reaction at each temperature was complete the reaction system would be cooled to room temperature and submitted to Temperature Programmed Oxidation (TPO) with 10% O_2 in He with a ramp rate of 10 °C/min up to 850 °C with a flow rate of 1 mL/s to determine the coke content and combustion profile. As shown in Figure 6, there is significant carbon deposited at 650 °C and very little at 800 °C. This agrees with the observed deactivation rate, suggesting a lower reaction temperature leads to greater carbon deposition and therefore faster catalyst deactivation.

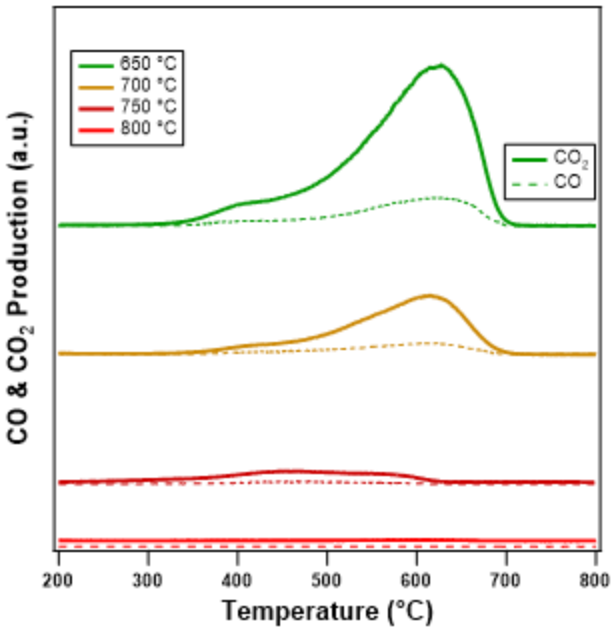

Figure 6. Temperature Programmed Oxidation of 10%Ni $Mg_2Al_2O_4$ and coke after 200 minutes on stream at 750, 700, 650, and 800 °C.

After the TPO the system would be reduced under hydrogen carried out at 850 °C for 30 minutes under 10% H_2 in He with a ramp rate of 10 °C/min and a flow rate of 1 mL/s. After 30 minutes at 850 °C the catalyst was switched to He and the next reaction temperature could be selected. As shown in Figure 7, the temperature-programmed reduction result shows with 10%Ni $Mg_2Al_2O_4$ that most of the Ni is interacting with the surface, a small amount of bulk Ni is seen on repeated runs which suggests Ni dispersion is slowly decreasing.

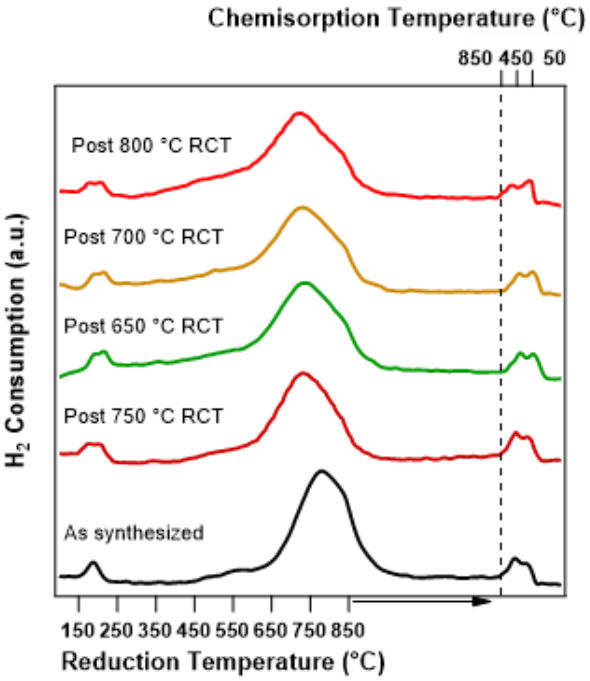

Figure 7. Temperature Programmed Reduction of 10%Ni $Mg_2Al_2O_4$ at up to 850 °C after oxidation of the catalyst prior to dry reforming at 750, 700, 650 and 800 °C.

Impact of water

There are significant changes in 10%Ni/$Mg_2Al_2O_4$ catalyst activity and stability at 700 °C when water is introduced, the middle panel with CO_2:CH_4:H_2O 1:1:0.5, as shown in Figure 8. As expected, the CO_2 conversion went down because the catalyst is now binding H_2O to the surface. The system returns to dry methane reforming and within error similar performance of the catalyst is seen after 2 hours without water.

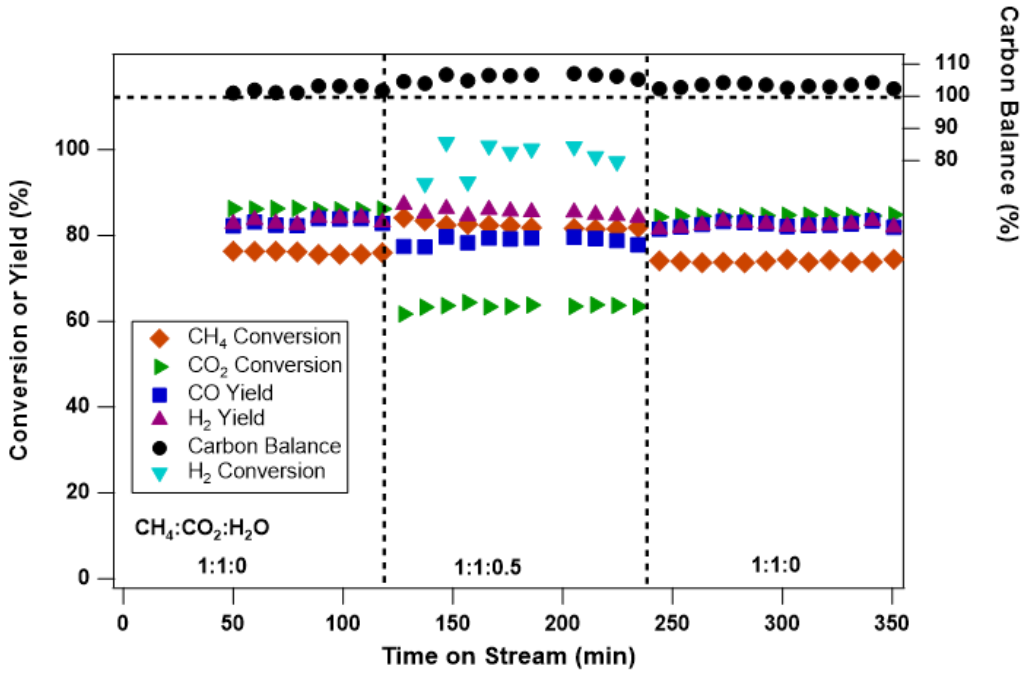

Figure 8. Reaction 10%Ni $Mg_2Al_2O_4$ with CH_4:CO_2 1:1 with and without water (0, 0.5, 0) dry reforming at 750 °C.

As shown in Figure 9 and 10, water increases the deactivation rate relative to dry conditions with 10%Ni/$Mg_2Al_2O_4$ catalyst except with the first time the test is run at 750 °C, by the time we run 750 °C a second time we see the deactivation. Once water is introduced, we see hydrogen yields increase and both CO yields and CO_2 conversion reduced.

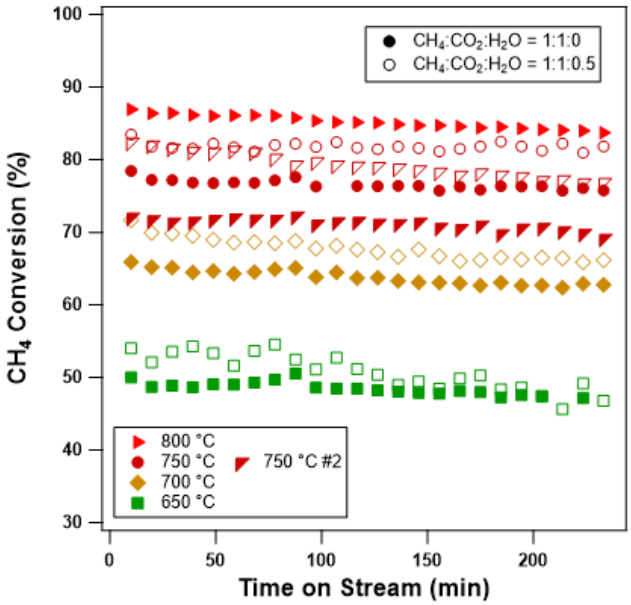

Figure 9. Reaction 10%Ni $Mg_2Al_2O_4$ with CH_4:CO_2 1:1 with and without water (0, 0.5) dry reforming at 750, 700, 650, 800, and 750 °C.

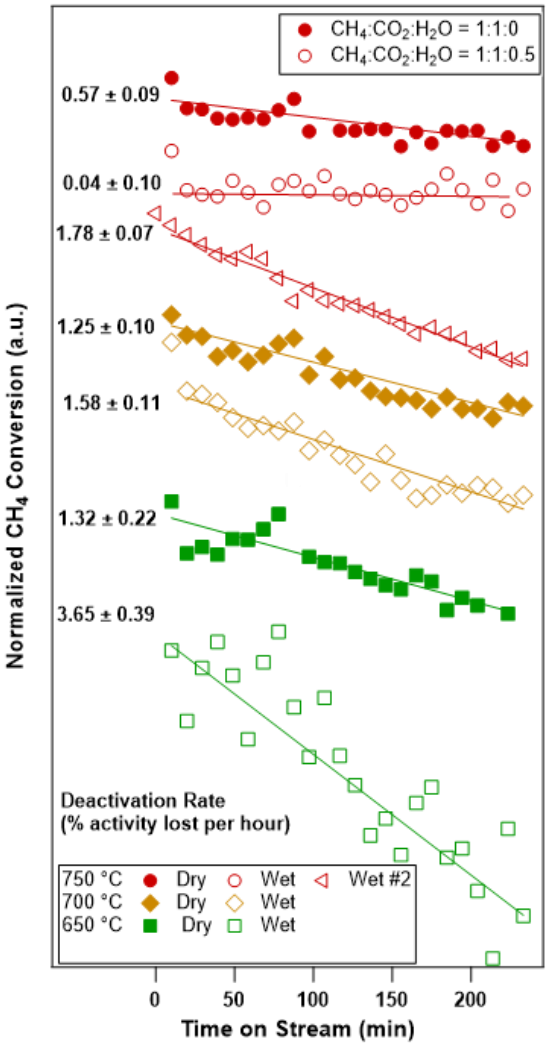

Figure 10. Normalized CH_4 conversion over 200 minutes to show deactivation of 10%Ni $Mg_2Al_2O_4$ with CH_4:CO_2 1:1 with and without water (0, 0.5) at 750, 700, 650, 800, and 750 °C.

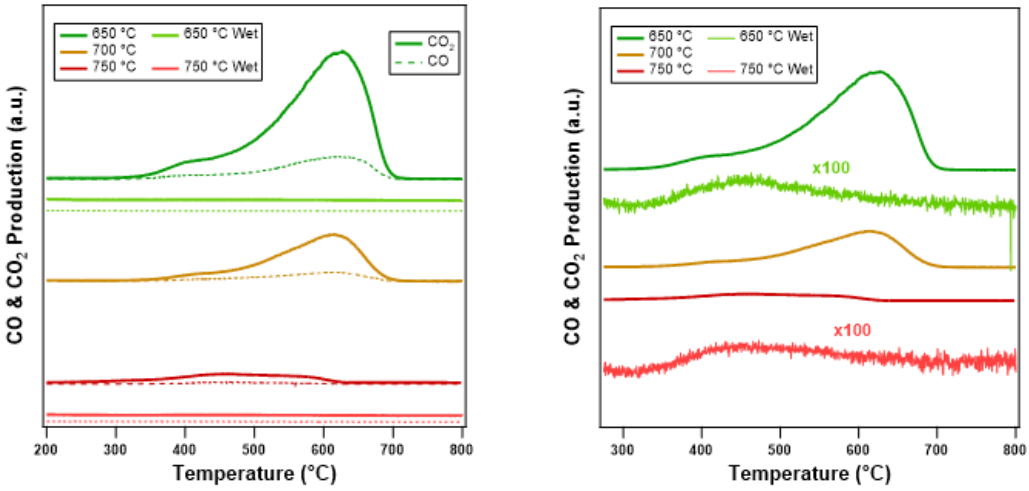

Figure 11. Temperature Programmed Oxidation of carbon deposits on 10%Ni $Mg_2Al_2O_4$ with CH_4:CO_2 1:1 with and without water (0, 0.5) 750, 700, and 650 °C.

Carbon deposition in the CO_2:CH_4:H_2O 1:1:0.5 runs with 10%Ni $Mg_2Al_2O_4$ catalyst is dramatically reduced as shown by the TPO runs, Figure 11. Together with the faster deactivation of the catalyst with water at CO_2:CH_4:H_2O of 1:1:0.5, we proposed the hypothesis that water may induce catalyst deactivation by oxidation of Ni or formation of hydroxide form. Therefore, CO_2:CH_4:H_2O 1:1:0.5 was perhaps too much water and we looked at the lower ratio of CO_2:CH_4:H_2O 1:1:0.1.

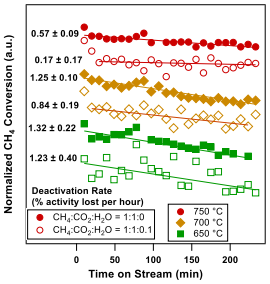

Figure 12. Normalized CH_4 conversion over 200 minutes to show deactivation of 10%Ni $Mg_2Al_2O_4$ with CH_4:CO_2 1:1 with and without water (0, 0.1) at 750, 700, and 650 °C.

In Figure 12, we observe that 10%Ni/$Mg_2Al_2O_4$ with CH_4:CO_2 1:1 with and without water (0, 0.1) at 750, 700, and 650 °C that the deactivation rates are reduced at all tested temperatures. Figure 11 is in contrast to Figure 9 where with larger amounts of water (CO_2:CH_4:H_2O 1:1:0.5) we saw increased deactivation with water at 650, 700, and 750 °C. It is hypothesized that higher water partial pressure (20%) suppresses carbon

deposits but promotes deactivation at all temperatures via additional deactivation mechanism. While the lower water partial pressure (5%) promotes increased catalyst stability and this is more noticeable at higher temperatures.

The 10%Ni/$Mg_2Al_2O_4$ with CO_2:CH_4:H_2O 1:1:0.5 at 750 °C has a variance equal to the value and was re-run over 12 hours.

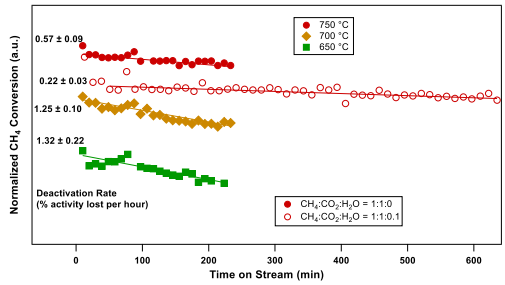

Figure 13. Normalized CH_4 conversion over 720 minutes to show deactivation of 10%Ni $Mg_2Al_2O_4$ with CH_4:CO_2 1:1 with water (0.1) at 750 °C.

The deactivation of 10%Ni $Mg_2Al_2O_4$ with CH_4:CO_2 1:1 with water (0.1) at 750 °C shown in Figure 13 has a deactivation rate that is significantly less than without water and the value is above the noise.

The Temperature Programmed Oxidation of the carbon deposits built up during 200 minutes of reacting 10%Ni/$Mg_2Al_2O_4$ with CH_4:CO_2 1:1 with water (0.1) shows essential no CO_2 or CO oxidation similar to Figure 11.

All these results strongly suggest that low partial pressure of water co-feeding, such as CO_2:CH_4:H_2O 1:1:0.1, suppressed carbon deposition and did not introduce new deactivation modes of the catalyst, and eventually led to a much improved catalyst stability.

Impact of Ni loading and the secondary metal
We also prepared a 5 wt% Ni/$Mg_2Al_2O_4$ catalyst and controls and tested it at 650 and 750 °C, CO_2:CH_4:1:1 with no water and approximately normalized for the amount of Ni by doubling the amount of 5 wt% Ni $Mg_2Al_2O_4$ relative to 10%Ni $Mg_2Al_2O_4$ catalyst, see Figure 14.

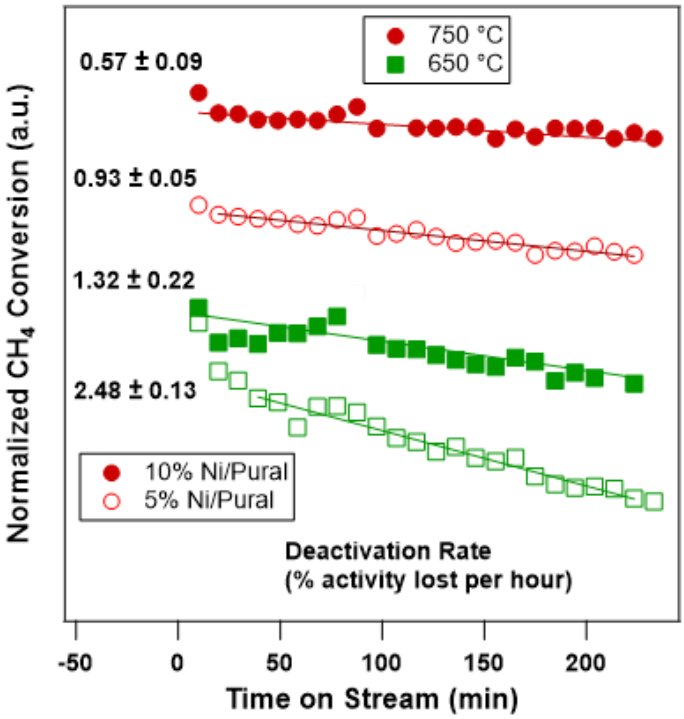

Figure 14. Normalized CH_4 conversion to indicate deactivation over 200 minutes with 5% Ni $Mg_2Al_2O_4$ and 10%Ni $Mg_2Al_2O_4$ with CH_4:CO_2 1:1 without water at 750, and 650 °C.

Interestingly while Ni loading was reduced twofold in 5% Ni/$Mg_2Al_2O_4$ with the working hypothesis that the Ni dispersion might increase or the Ni particle size would be reduced to provide a more active catalyst, the 5% Ni/$Mg_2Al_2O_4$ results show in dry reforming the 5% Ni/$Mg_2Al_2O_4$ deactivates faster than the 10% Ni $Mg_2Al_2O_4$.

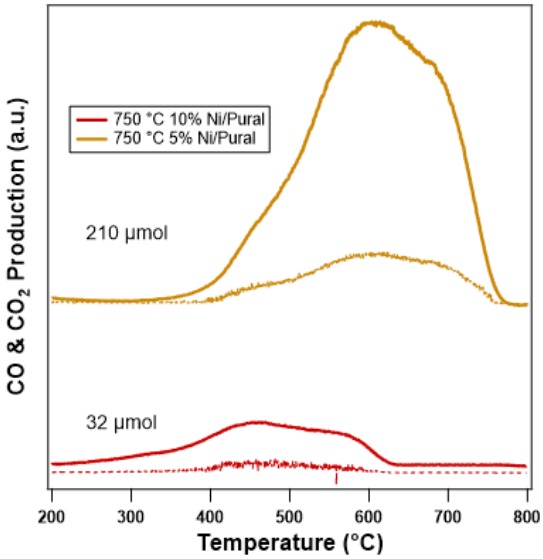

Figure 15. Temperature Programmed Oxidation of 5% Ni $Mg_2Al_2O_4$ and 10%Ni $Mg_2Al_2O_4$ of carbon deposits after dry reforming for 200 minutes with CH_4:CO_2 1:1 without water at 750, and 650 °C.

Figure 15 shows that the 5% Ni $Mg_2Al_2O_4$ appears to generate more carbon deposits at 750 °C during dry methane reforming than 10%Ni $Mg_2Al_2O_4$ which is consistent with a faster deactivation rate.

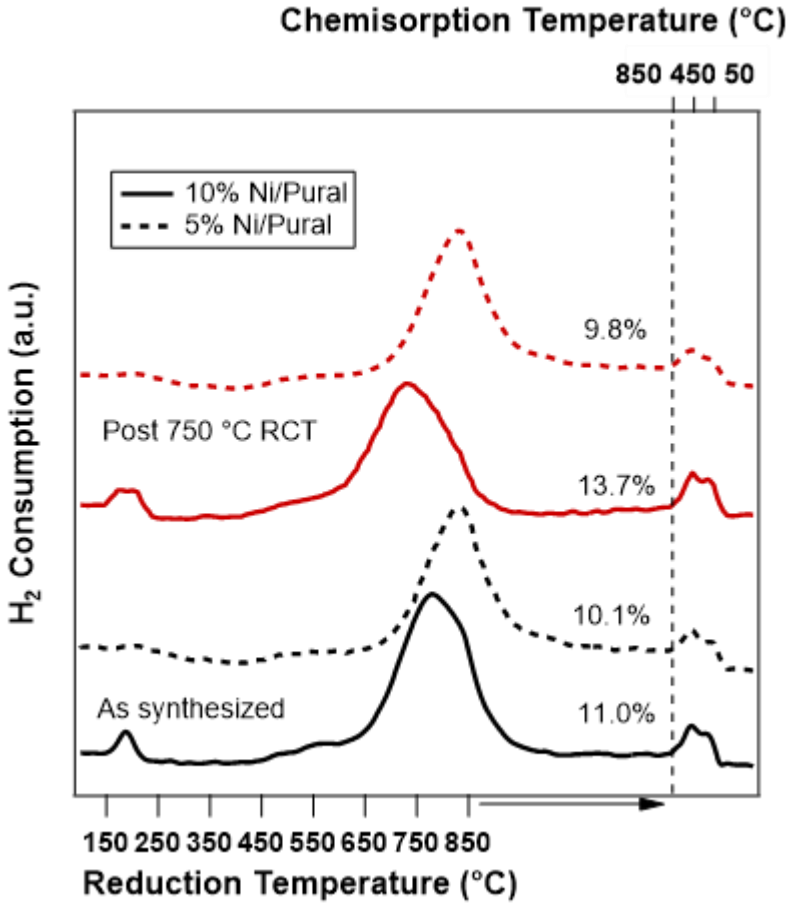

Figure 16. Temperature Programmed Reduction of 5% Ni $Mg_2Al_2O_4$ and 10%Ni $Mg_2Al_2O_4$ with H_2 prior to dry methane reforming at 750, and 650 °C.

From the TPR in Figure 16, the Ni dispersion look similar for 5% Ni $Mg_2Al_2O_4$ and 10%Ni $Mg_2Al_2O_4$.

We also prepared a 5 wt% Ni + 5% Co $Mg_2Al_2O_4$ catalyst and controls and tested it at 750 °C, CO_2:CH_4:1:1 with no water. The hypothesis was the Co would bind the oxygenated species and the nickel would bind the methyl groups to facilitate a spillover reaction and a stable catalyst.

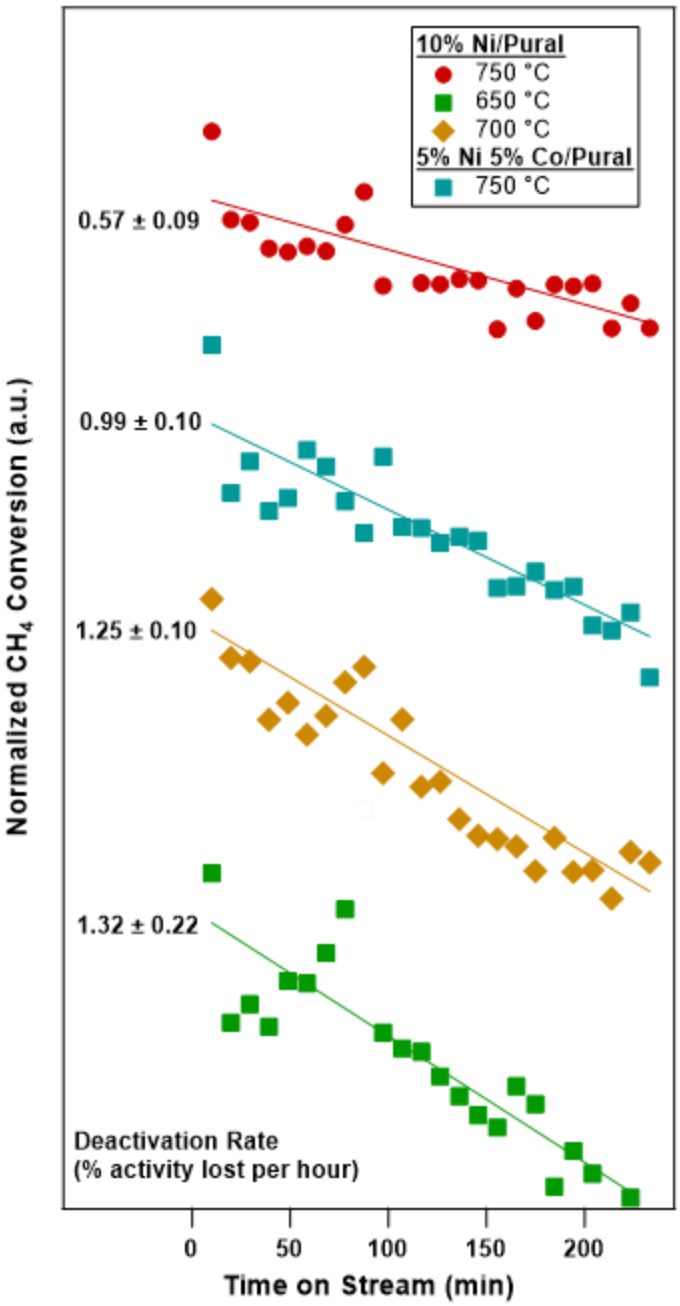

Figure 17. Normalized CH_4 conversion to indicate deactivation over 200 minutes with 5% Ni 5% Co $Mg_2Al_2O_4$ and 10%Ni $Mg_2Al_2O_4$ with CH_4:CO_2 1:1 without water at 750 °C.

Figure 17 shows that 5% Ni 5%-Co/$Mg_2Al_2O_4$ appears to deactivate at 750 °C during dry reforming faster than 10%Ni/$Mg_2Al_2O_4$.

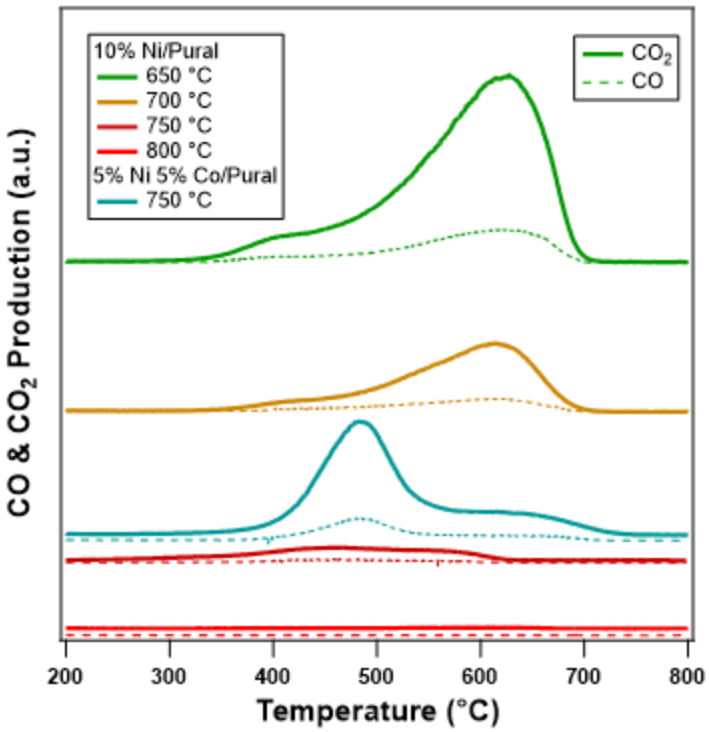

Figure 18. Temperature Programmed Oxidation of 5% Ni 5% Co $Mg_2Al_2O_4$ and 10%Ni $Mg_2Al_2O_4$ of carbon deposits after dry reforming for 200 minutes with CH_4:CO_2 1:1 without water at 750 °C.

In Figure 18 comparing the 5% Ni 5%-Co/$Mg_2Al_2O_4$ TPO with the on 10%Ni $Mg_2Al_2O_4$ TPO at 750 °C there is significantly more carbon deposits. Additionally, from the TPO of carbon deposits in Figure 17 it is shown that the 5% Ni 5% Co $Mg_2Al_2O_4$ has distinct carbon deposits, that is have a significant population that is more easily oxidized than the carbon deposits on 10%Ni $Mg_2Al_2O_4$.

We also prepared a 5% Ni-5%Ce/$Mg_2Al_2O_4$ catalyst and controls and tested it at 650 and 750 °C, CO_2:CH_4:1:1 with no water. The loading of the catalysts was on a nickel basis and there was 60 mg of 5% Ni 5% Ce $Mg_2Al_2O_4$ in the reactor and 30 mg of 10%Ni $Mg_2Al_2O_4$ in the reactor. The hypothesis was that Ce would improve the CO_2 absorption and the amount of surface-active Ni sites.

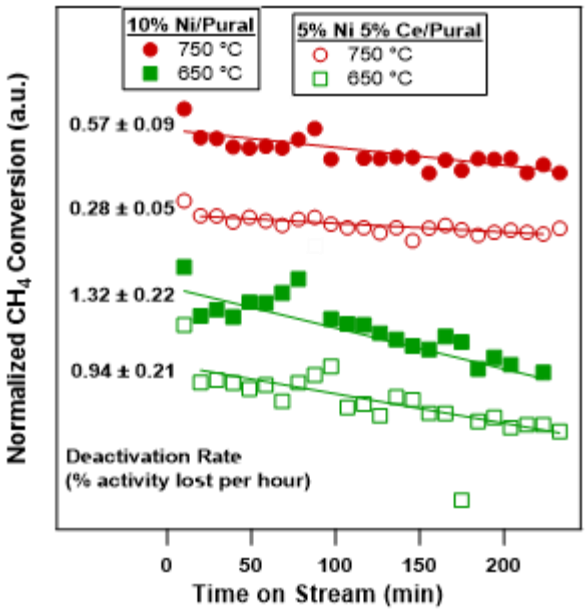

Figure 19. Normalized CH_4 conversion to indicate deactivation over 200 minutes with 5% Ni 5% Ce $Mg_2Al_2O_4$ and 10%Ni $Mg_2Al_2O_4$ with CH_4:CO_2 1:1 without water at 650 and 750 °C.

Figure 19 indicates that the Ce in 5% Ni 5% Ce $Mg_2Al_2O_4$ improves the catalyst stability at 650 and 750 °C relative to 10%Ni/$Mg_2Al_2O_4$ by approximately 29% and 51% respectively, under dry reforming conditions.

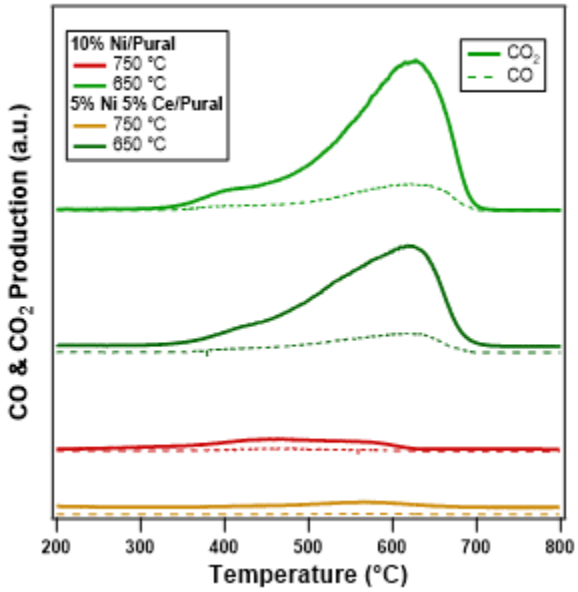

Figure 20. Temperature Programmed Oxidation of 5% Ni 5% Ce $Mg_2Al_2O_4$ and 10%Ni $Mg_2Al_2O_4$ of carbon deposits after dry reforming for 200 minutes with CH_4:CO_2 1:1 without water at 650, and 750 °C.

Figure 20 shows that 5% Ni 5% Ce $Mg_2Al_2O_4$ decreases carbon deposits relative to 10%Ni $Mg_2Al_2O_4$ at 650 and 750 °C by approximately 27% and 66%, respectively under dry reforming conditions.

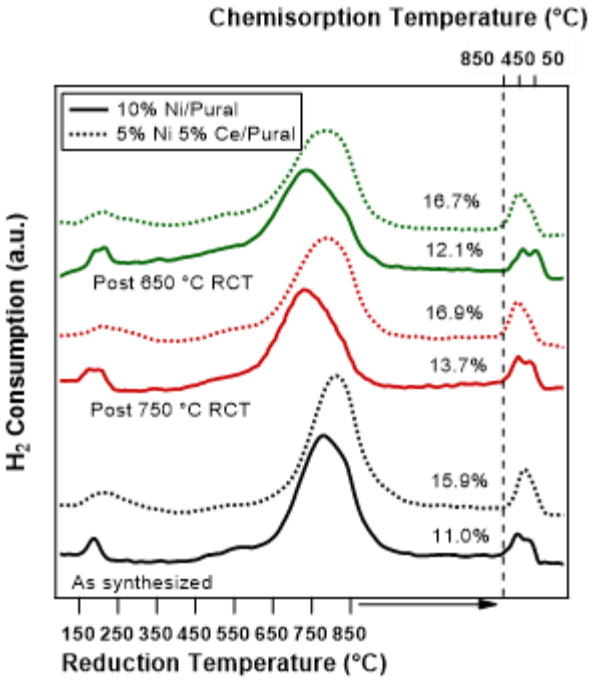

Figure 21. Temperature Programmed Reduction of 5% Ni 5% Ce $Mg_2Al_2O_4$ and 10%Ni $Mg_2Al_2O_4$ with H_2 prior to dry methane reforming at 750, and 650 °C.

The TPR in Figure 21, appears to illustrate the 5% Ni 5% Ce/$Mg_2Al_2O_4$ has increased dispersion of the Ni relative to 10%Ni $Mg_2Al_2O_4$ however, at this stage we can not say whether this is due to the particle size of the Ni effect or the interaction of the Ni with the ceria.

Task 3: Simulation of the complex catalytic system

Baseline Multisite Mean Field Thermodynamic Model of Combined Dry and Steam Reforming over Ni/$MgAl_2O_3$-Based Catalysts

To guide and rationalize the design of combined dry and steam reforming catalysts based on a magnesium aluminate ($MgAl_2O_3$) supported Ni formulation, a baseline thermodynamic model was constructed. The underlying thermodynamics of this model are represented explicitly by a mean field treatment of the free energy of the surface system, F_{surf}, which is a summation of free energy contributions from key reforming intermediates that occupy the multiple types of sites available on this catalyst. As a baseline approximation, we neglect lateral interactions between adspecies, which can be added later as needed. However, site blocking due to co-adsorption of multiple intermediates is fully represented. With these considerations, the free energy of the surface system is given by equation 1:

$$F_{surf}(\{\theta_{iX}\}) = \sum_{i}^{(species)} \sum_{X}^{(site\ types)} \left(\sigma_{iX}\left[V_{iX} - TS_{iX}^{(approx)}\right] - k_B T ln[\Omega_{iX}]\right) \quad (1)$$

where σ_{iX} and V_{iX} are the areal coverage (number of species per unit surface area) and formation energy of intermediate species i when occupying a site of type X, respectively;

T is the absolute temperature; $S_{iX}^{(approx)}$ is the *local* entropy of this species (which is currently being approximated in this baseline model, but can be computed from quantum mechanical first principles in future refinements of the model); and Ω_{iX} is the *global* entropy provided by each species. This global entropy term accounts for the increased/decreased space available due to co-adsorption of the other adspecies, i.e., site blocking. A full derivation will be provided in future publications, but the final functional form of this term is given as

$$\Omega_{iX} = \left[\frac{\left(f_X - \sum_{jY \neq iX} b_{iX,jY}\theta_{jY}\right)^{\left(f_X - \sum_{jY \neq iX} b_{iX,jY}\theta_{jY}\right)}}{(\theta_{iX})^{(b_{iX,iX}\theta_{iX})}\left(f_X - \sum_{jY} b_{iX,jY}\theta_{jY}\right)^{\left(f_X - \sum_{jY} b_{iX,jY}\theta_{jY}\right)}} \right]^{\frac{n_S N_{u.c.}}{b_{iX,iX}}} \quad (2)$$

where n_S is the total number sites per surface unit cell; f_X is the fraction ($0 \leq f_X \leq 1$) of the surface covered in sites of type X; θ_{iX} is site coverage, i.e., the fraction of X sites occupied by species i (number of species i per total number of X sites, equivalent to $\theta_{iX} = \frac{\sigma_{iX}}{n_S}$); $b_{iX,jY}$ is the number sites of type X (that could be occupied by species i) that are blocked when a species j occupies a site of type Y; and $N_{u.c.}$ is the number of nominal unit cells making up the material's surface. Equation 1 is always taken to the thermodynamic limit where $N_{u.c.}$ and $n_S N_{u.c.}$ approach infinity.

Modeling the free energy as in Equation 1 means that instead of taking the surface to be made up of a homogenous distribution of a single site type (often denoted with an asterisk, "*", in the literature), the Ni^0 sites, Ni-support interface sites, perimeter-adjacent Mg sites, and perimeter-adjacent (Al)O sites are represented within the model as separate entities. To determine the relative abundance of each site type in any given model, we compute the number of each type of site that would exist given a hemispherical Ni nanoparticle (with the area of surface unit cells equivalent to that of Ni(111)) supported on a nominally flat terrace of the support, see **Figure 22** for the conceptual topology of this system

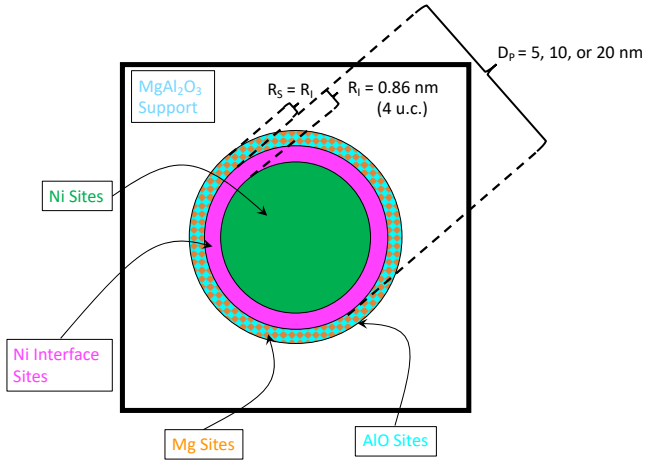

Figure 22. Top-down view of the conceptual topology of the Ni/$MgAl_2O_3$ catalyst system used to determine the relative preponderance of the four site types represented in the multisite thermodynamic model developed for this project. Particle diameter (D_p), interface depth (R_I), and support perimeter depth (R_S) are treated as parameters.

By varying the nanoparticle size/diameter, a realistic variety of site ratios can be modeled to determine the effect of particle size and relative abundance and distribution of intermediates.
The formation energy of each intermediate occupying each site type, V_{iX}, is found from first principles DFT calculations of bound intermediates and is given by Equation 3:

where E_{iX}^{DFT}, E_{slab}^{DFT}, E_{C}^{DFT}, E_{O}^{DFT}, and E_{H}^{DFT} are the DFT-computed electronic energies of the system, pristine surface, a carbon atom, oxygen atom, and hydrogen atom, respectively; and N_C, N_O, N_H, are the number of carbon, oxygen, and hydrogen atoms, respectively, making up the bound intermediate, i, whose formation energy at a site of type X is being computed. Currently, this value is taken at the limit of infinite dilution (the so called "zero-coverage" limit), but terms for finite-concentration effects can be added to this energy in future refinements of the models. Two molecular models, shown in **Figure 23,** were constructed to compute the formation energies, V_{iX}, of each intermediate occupying the four site types present within this model using ab initio density functional theory (DFT) calculations.

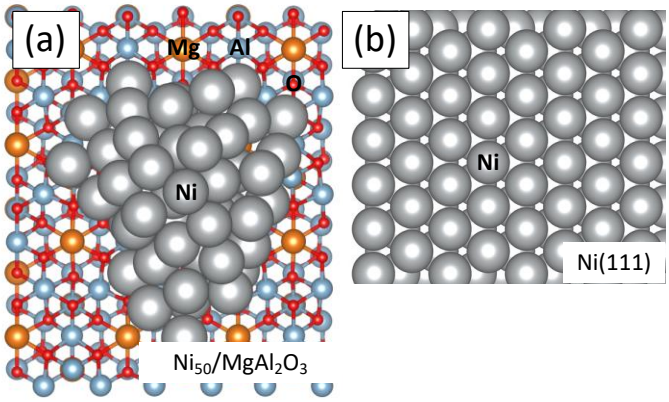

Figure 23. Top-down views of the two molecular models used in computation, via density functional theory, of the formation energies of intermediates. (a) An amorphous Ni_{50} nanoparticle supported on a $MgAl_2O_3$ surface, which was used to compute formation energies at Ni-support interface, Mg, and (Al)O sites. (b) The Ni(111) surface used to compute the formation energies at Ni^0 sites. Spheres in grey, orange, blue, and red, represent Ni, Mg, Al, and O atoms, respectively.

Figure 24 shows these values for each of the primary intermediates involved in dry and steam reforming of methane that we represent in the model. The intermediates' formation energies at each site type are shown as separate-colored bars, with more negative values

$$V_{iX} = E_{iX}^{DFT} - E_{slab}^{DFT} - N_C E_C^{DFT} - N_O E_O^{DFT} - N_H E_H^{DFT} \quad (3)$$

indicating greater stability at that type of site. However, it should be noted that one cannot compare stability between non-isomeric intermediates in this chart.

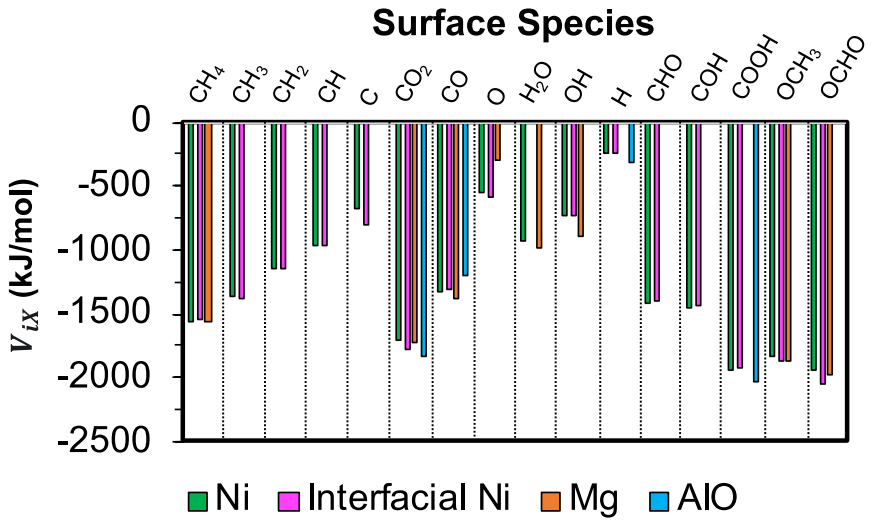

Figure 24. Computed formation energies of dry and steam reforming of methane intermediates bound at the four site types represented in this model.

Finally, we expose the model to a reservoir with constant partial pressures of CH_4, CO_2, CO, H_2, and H_2O. In our baseline model, the CO_2:CH_4 ratio is maintained at 1:1 and H_2O:CO_2 ratios of 0:1 and 0.5:1 were tested. CO_2 and H_2O conversions were used to compute these partial pressures, and standard state chemical potentials were computed from NIST database.

The high dimensionality of Equation 1 means that minimization of the total free energy of the surface/reservoir system is a non-trivial task. We are actively working on applying an artificial bee colony ("swarm intelligence") global minimization scheme to ensure that we are finding the global minimum instead of merely a local minimum in the free energy. Here, we have employed a simple generalized gradient algorithm to minimize the free energy which provides reasonable equilibrium solutions that are well suited as a proof of concept despite not guaranteeing a global minimum solution. The resulting site coverage distributions are shown in **Figure 25** for three nanoparticle diameters (5, 10, and 20 nm) and two sets of reservoir conditions (no H_2O and low CO_2 conversion; and a 0.5:1 H_2O to CO_2 ratio with near-equilibrium CO_2 conversion). The most obvious feature of these results is the near-to-complete hydroxylation of the exposed O atoms at the Ni-support perimeter (AlO sites, light blue bars in **Figure 25**) regardless of the nanoparticle size or reservoir conditions. This implies that the support acts a hydrogen sink in the zero-coverage limit. Even if complete hydroxylation is kinetically limited (which a future kinetic model will reveal, this would represent a major thermodynamic driving force during the reforming reaction. Hydroxylation of the exposed Mg sites (orange bars) is also a major feature that qualitatively appears to decrease as particle size increases with CO or H_2O replacing the OH groups. CO is less concentrated on the Ni^0 sites as the particle size increases as well. This should be considered undesirable since CO is bound more tightly to Mg sites than to Ni^0 or Ni interface sites (see **Figure 24**) and would thus be much slower to desorb as product. This highlights the importance of ensuring a small and monodisperse distribution of Ni nanoparticle sizes. Qualitatively, we also see that the total

distribution of intermediates is smaller on smaller nanoparticles, suggesting that smaller nanoparticles allow more control over the species formed.

Another very interesting feature in **Figure 25** is the absence of C or CH species. Due to the large thermodynamic driving force provided by carbide formation and coking, these processes have been neglected here (the model would simply predict that the equilibrium state of the Ni nanoparticle is completely deactivated). It is surprising then that the intermediates species to deactivation (C and CH) are not thermodynamically favored. This implies that the active Ni catalyst is metastable with respect to coking and carbide formation with deactivation a kinetically controlled process. In other words, there is a kinetic gap between the active metastable state and inactive state occupying the bottom of the thermodynamic well. This is in fact very good news from the perspective of designing stable dry reforming catalysts since reaction kinetics can in principle be tuned to maintain this gap. If this feature holds in future refinement of the thermodynamic model, it implies that deactivation may be largely avoidable.

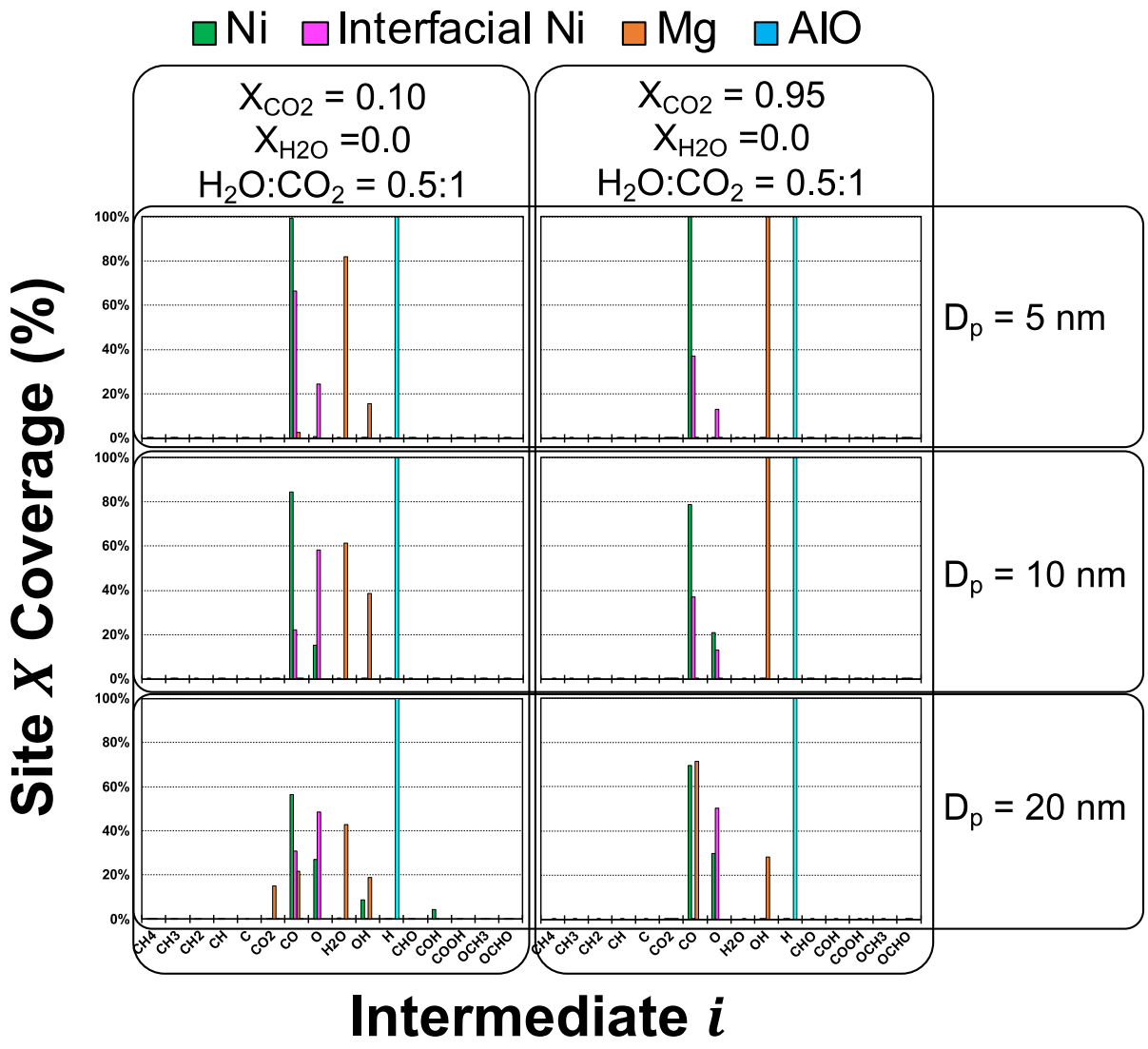

Figure 25. Thermodynamic equilibrium site coverages (y-axes) for each dry and steam reforming intermediate (x-axes) at each of the four site types (colored bars) represented in the thermodynamic model developed here. Each graph represents a model based on a Ni nanoparticle diameter of those shown to the right, while the corresponding reservoir conditions—CO_2 conversion, H_2O conversion, and $H_2O:CO_2$ ratios— are shown above.

The results of this baseline model strongly motivate the need for thorough and careful modeling of dry and steam reforming microkinetics. A high-fidelity microkinetic model incorporating the details made accessible by our thermodynamic model can be used to guide experimental design to hasten the development of a stable dry reforming catalyst. It is worth noting that one of the strengths of our approach to modeling the thermodynamics of this process here is its direct transferability to the kinetic system. Since chemical potentials of the reaction intermediates are needed to define the extents of reaction and rate expressions, we need only differentiate the free energy defined in Equation 1 with respect to differential changes in each species' coverages at each site

type to provide the ingredients needed for its corresponding microkinetic model. This will be the approach used to design and deliver our kinetic model milestone in future work.

Conclusions

It would appear that the partial pressure of water and the temperature of the reaction are very important for CO_2 reforming of CH_4. Figure 26 shows lower temperatures of reaction increase the rate of deactivation with the formation of more deposited carbon. As to the water partial pressure, a small amount of water (0.1) decreases the deactivation with decreasing carbon deposition. However, higher partial pressure of water (0.5) increases the deactivation rate of the 10%Ni $Mg_2Al_2O_4$ catalyst, likely because of the deactivation of Ni sites due to the formation of NiO on either surface or bulk.

Figure 26 Preliminary thoughts on observations of reactions with and without water

The most stable conditions for 10 %Ni $Mg_2Al_2O_4$ catalyst were obtained with smaller amounts of water (0.1) and higher temperatures (750 °C).

The addition of the 5wt% Ce co-catalyst with 5% Ni $Mg_2Al_2O_4$ has shown a> 20% reduction in the deactivation rate at 650 and 750 °C for methane reforming of CO_2 relative to the baseline 10%Ni $Mg_2Al_2O_4$.

The end of year milestone was:
By end of the year show two strategies (cocatalysts, with and without water) that reduce the carbon deposition rates by 20% relative to the baseline Ni MgAlO at < 800 C. This means at 650-750 °C that the technical feasibility of the concept is shown. (September 2021).

We have demonstrated that, with the inclusion of 5% H_2O, the 10%Ni $Mg_2Al_2O_4$ catalyst at 650, 700, and 750 °C showed a > 20% reduction in carbon deposits. The addition of the 5 wt% Ce co-catalyst with 5% Ni/$Mg_2Al_2O_4$ has shown a > 20% reduction in the deactivation rate at 650 and 750 °C for methane reforming of CO_2 relative to the baseline 10%Ni/$Mg_2Al_2O_4$.

Table 4. Performance of catalyst systems relative to the 10%Ni $Mg_2Al_2O_4$ catalyst baseline and the end of year milestone:

Stabilizing Strategy	Temperature (°C)	Percent decrease in carbon formation rate	Percent decrease in deactivation rate
Ceria Addition	750	66%	51%
Ceria Addition	650	27%	29%
Water Addition (5%)	750	100%	70%
Water Addition (5%)	700	100%	33%
Water Addition (5%)	650	100%	6.8%

The modeling highlights the importance of ensuring a small and monodisperse distribution of Ni nanoparticle sizes. Experimentally the hypothesis that smaller Ni particles are more reactive for methane reforming of CO_2 and stable with regard to both carbon deposits deactivation and deactivation due to sintering of the Ni particles has yet to be determined.

The results of this baseline model strongly motivate the need for thorough and careful modeling of dry and steam reforming microkinetics and experimentally the next phase would be to start determining the kinetics of a dilute reaction system with small amounts of water and cerium as a cocatalyst.

Acknowledgements

The authors gratefully acknowledge funding for this research provided by the Energy & Environment Directorate FY 2021 Laboratory Directed Research and Development (LDRD) seed call. This work was done at the Pacific Northwest National Laboratory (PNNL) which is a multi-program national laboratory operated by Battelle for DOE under contract DE-AC05-76RL01830. Finally, the authors wish to thank Karthi Ramasamy, Vanessa Lebarbier Dagle and Robert Dagle for invaluable consultation, and access to resources.

References

1. As described by DOE Funding Opportunity Announcement Fossil Energy Based Production, Storage, Transport and Utilization of Hydrogen Approaching Net-Zero or Net-Negative Carbon Emissions DE-FOA-00024000 advanced gasification technologies are those capable of improved performance, reliability, and flexibility to produce net

zero- or negative-carbon hydrogen by readily accommodating integration of pre-combustion carbon capture, and providing capability to utilize low cost and negative-cost feedstock materials along with traditional feedstocks to produce low-cost net-zero carbon fuels and chemicals.

2. Methane dry reforming over Ni/Mg-Al-O: On the significant promotional effects of rare earth Ce and Nd metal oxides. Fang, X.; Zhang, J.; Liu, J.; Wang, C.; Huang, Q.; Xu, X.; Peng, H.; Liu, W.; Wang, X.; Zhou, W. Journal of CO_2 Utilization 25 (2018) 242–253.

3. Biogas reforming of carbon dioxide to syngas production over Ni-Mg-Al catalysts. Zhana, Y.; Hana, J.; Bao, Z.; Cao, B.; Li, Y.; Streete, J.; Fei Yua, F. Molecular Catalysis 436 (2017) 248–258.

4. High-Performance Bimetallic Catalysts for Low-Temperature Carbon Dioxide Reforming of Methane. Muhammad Aziz, A. A.; Setiabudi, H. D.; Teh, L. P.; Asmadi, M.; Matmin, J.; Wongsakulphasatch, S. Chem. Eng. Technol. 2020, 43, No. 4, 661–671.

5. Understanding the role of Ni-Sn interaction to design highly effective CO_2 conversion catalysts for dry reforming of methane. Guharoy, U.; Le Saché, E.; Cai, Q.; Ramirez Reina, T.; Gu, S. Journal of CO_2 Utilization 27 (2018) 1–10

6. Highly stable and active catalyst for hydrogen production from biogas. Serrano-Lotina,A.; Daza, L; Journal of Power Sources 238 (2013) 81-86.

7. Steam/CO_2 Reforming of Methane. Carbon Filament Formation by the Boudouard Reaction and Gasification by CO_2, by H_2, and by Steam: Kinetic Study. J.-W. Snoeck, J.-W.; Froment, G. F.; Fowles, M. Ind. Eng. Chem. Res. 2002, 41, 4252-4265.

8. Long-term stability test of Ni-based catalyst in carbon dioxide reforming of methane. A. Serrano-Lotina, A.; Daza, L. Applied Catalysis A: General 474 (2014) 107–113.

9. Catalytic Dry Reforming of Methane: Insights from Model Systems. Wittich, K.; Krämer, M.; Bottke N.; Schunk, S. A. ChemCatChem 2020, 12, 2130–2147.

10. Carbon gasification from Fe–Ni catalysts after methane dry reforming. Theofanidis, S. A.; Batchu, R.; Galvita, V. V.; Poelman, H.; Marin, G. B. Applied Catalysis B: Environmental 185 (2016) 42–55.

11. Surface Reaction Kinetics of Steam- and CO_2-Reforming as Well as Oxidation of Methane over Nickel-Based Catalysts. Herrera Delgado, K.; Maier, L; Tischer, S; Zellner, A.; Stotz, H.; Deutschmann, O. Catalysts 2015, 5, 871-904.

12. Steam Reforming of Methane Over Nickel: Development of a Multi-Step Surface Reaction Mechanism. L. Maier, L.; Schädel, B.; Herrera Delgado, K.; Tischer, S.; Deutschmann, O. Topics in Catalysis 54, 845 (2011) 845-858.

13. Tuning combined steam and dry reforming of methane for “metgas” production: A thermodynamic approach and state-of-the-art catalysts. Jabbour, K. Journal of Energy Chemistry 48 (2020) 54–91.

14. Microkinetics Modeling of Catalytic Converters. Sriramulu, S.; Moore, P. D.; Mello, J. P.; Weber, R. S. SAE 2001-01-0936.

15. Structure sensitivity and its effect on methane turnover and carbon co-product selectivity in thermocatalytic decomposition of methane over supported Ni catalysts Xu, M.; Lopez-Ruiz, J. A.; Kovarik, L.; Bowden, M. E.; Davidson, S. D.; Weber, R. S.; Wang, I.-W.; Hu, J.; Dagle, R.A. Applied Catalysis A; General, 611 (2021) 117967.

16. Methane and ethane steam seforming over $MgAl_2O4$ -supporrted Rh and Ir catalysts: Catalytic Implications for natural gas reforming application Lopez, J. S.; Lebarbier Dagle, V.; Deshmane, C. A.; Kovarik, L.; Wegeng, R. S.; Dagle, R. A. Catalysts, 2019, 9, 801. Doi:10.3390/catal9100801

Pacific Northwest National Laboratory

902 Battelle Boulevard
P.O. Box 999
Richland, WA 99354
1-888-375-PNNL (7665)

www.pnnl.gov